

Research Article

Automated Waterline Detection in the Wadden Sea Using High-Resolution TerraSAR-X Images

Stefan Wiehle and Susanne Lehner

DLR Maritime Security Lab, Henrich-Focke-Straße 4, 28199 Bremen, Germany

Correspondence should be addressed to Stefan Wiehle; stefan.wiehle@dlr.de

Received 8 January 2015; Revised 25 March 2015; Accepted 1 April 2015

Academic Editor: Armando Marino

Copyright © 2015 S. Wiehle and S. Lehner. This is an open access article distributed under the Creative Commons Attribution License, which permits unrestricted use, distribution, and reproduction in any medium, provided the original work is properly cited.

We present an algorithm for automatic detection of the land-water-line from TerraSAR-X images acquired over the Wadden Sea. In this coastal region of the southeastern North Sea, a strip of up to 20 km of seabed falls dry during low tide, revealing mudflats and tidal creeks. The tidal currents transport sediments and can change the coastal shape with erosion rates of several meters per month. This rate can be strongly increased by storm surges which also cause flooding of usually dry areas. Due to the high number of ships traveling through the Wadden Sea to the largest ports of Germany, frequent monitoring of the bathymetry is also an important task for maritime security. For such an extended area and the required short intervals of a few months, only remote sensing methods can perform this task efficiently. Automating the waterline detection in weather-independent radar images provides a fast and reliable way to spot changes in the coastal topography. The presented algorithm first performs smoothing, brightness thresholding, and edge detection. In the second step, edge drawing and flood filling are iteratively performed to determine optimal thresholds for the edge drawing. In the last step, small misdetections are removed.

1. Introduction

The Wadden Sea is a very unique and dynamic region in the southeastern North Sea, expanding along the coasts of the Netherlands, Germany, and Denmark. Tidal flats extend up to 20 km away from the coast during low tide with features like extended tidal mudflats, tidal inlets, and sand banks. All these structures move and change their shape over time under the influence of tidal water currents transporting large amounts of eroded material. As an example, island Trischen, located about 10 km off the mainland, moves eastwards about 30 m per year. Heavy storms and storm surges can cause large variations in tidal inlet or sand bank extensions in very short time; a single storm can cause a magnitude of morphological changes equal to several months of fair-weather conditions [1].

All ship traffic to the largest German ports of Hamburg, Bremerhaven, and Wilhelmshaven has to cross the Wadden Sea. Hence, the observation of obstacles like sand banks and the decreasing of the water depth in this area are crucial for the maritime security. Conventional monitoring campaigns

with ships or airplanes are economically expensive and can only provide limited coverage. The evolution of the Wadden Sea as well as large river estuaries like Elbe and Weser can be efficiently monitored by detecting waterlines in high-resolution TerraSAR-X (TS-X) radar satellite data. In contrast to optical satellite data which achieve a comparable resolution and repetition time, synthetic aperture radar (SAR) data are independent of weather conditions. This not only allows reliable repeated acquisitions, but also is a necessity to see through the cloud cover during or directly after storms.

While waterline or coastline detection from SAR images is not a new task, the Wadden Sea poses additional challenges compared to usual coastlines without tidal flat areas. The Normalized Radar Cross Section (NRCS) σ_0 of the water surface in X-band SAR is dependent on wind field conditions [2]. Except for high sea state conditions, the contrast between water and dry sand, cliffs or grass in a SAR image is often high enough for separation based on brightness thresholding alone. Tidal mudflats, on the other hand, may possess a wide range of NRCS levels depending on factors like surface roughness and remaining surface water [3]. Particularly wet mud

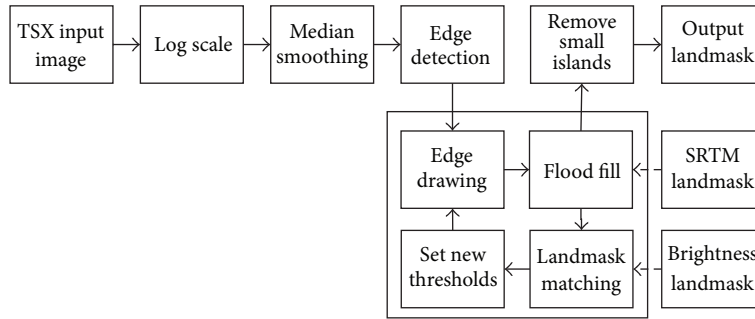


FIGURE 1: Flow chart of our presented algorithm. The steps of edge drawing and flood filling are repeated with adapted thresholds until a maximum of agreement to the brightness landmark is reached. The SRTM landmark helps to provide starting points for the flood filling.

flats yield only a very low NRCS due to a specular reflection of the radar beam. Hence, these areas usually appear darker in a SAR intensity image than the surrounding water, except for very low wind speeds when the water is also dark.

Most coastline detection algorithms presented previously do not cover the challenges of the Wadden Sea. Lee and Jurkevich [4] presented a method working on a single polarization image including several strong smoothing processes which are unsuitable for the small inlets in the Wadden Sea at low tide. For the often very dark mudflats, approaches primarily based on brightness segmentation (e.g., [5, 6]) are less applicable than for usual coastlines. Studies like Yu and Acton [7] use polarimetric SAR data which allow for an easier detection of water while Dellepiane et al. [8] use interferometric SAR acquisitions. Another approach is used by Gade et al. [9], where several SAR satellites working in different radar bands (L, C, X) are combined for monitoring and classification of mudflats. Although using polarimetric, interferometric, or even multiband SAR data does provide additional information to help with the coastline detection, most TS-X acquisitions are acquired in single polarization without interferometry; hence, our algorithm was developed to work on these settings. The construction of a digital elevation model (DEM) for intertidal zones was the focus of Mason and Davenport [10], who developed a semiautomatic method for coastline detection using a multiscale approach. Niedermeier et al. [11] also investigated coastlines in the German Bight area using a wavelet method and comparisons with optical data. However, while waterline extraction worked well on optical and SAR images, only the SAR images were used in their morphological study due to their reliable, weather independent coverage. A similar study was also conducted by Heygster et al. [12] for parts of Wadden Sea using ERS-SAR data.

We aim to extend these studies of [11, 12] using high-resolution TS-X data to determine the Wadden Sea topography. For this, an algorithm for waterline extraction was developed as a first step, which will further be used primarily for topography but also for landmark generation under Near Real Time (NRT) conditions. The algorithm is designed to work on single polarization SAR acquisitions of coasts with tidal flat areas. Its unique property is the combination of iterative edge drawing and flood filling yielding precise waterlines with a runtime suitable for NRT processing.

2. Waterline Extraction

Our algorithm accounts for the features of the Wadden Sea and solves the problem of waterline detection with a combination of edge detection, brightness thresholding, and a previously determined coarse landmark. The flow chart is shown in Figure 1 and described in the following paragraphs.

As the first step of our algorithm, the original TS-X input image is scaled logarithmically to increase the contrast in dark regions which appear in the sea and mudflats; the resulting reduced contrast in bright regions like cities or mainland structures is not significant for our purpose. In order to reduce speckle, the entire scene is smoothed in the next step. For good edge preservation, median smoothing is applied twice. For the smoothing window size, larger windows yield to better homogeneity and easier edge detection; however, structures smaller than the window like small tidal creeks are removed by the median filter. We found a good size of the smoothing window to be $(2n + 1) \times (2n + 1)$ with $n = 8/S$ and $n \geq 1$, where S is the scaling factor. When the full TS-X scene is scaled down by a factor of $S = 4$ before processing, this yields a 5×5 smoothing window.

The next step is to run an edge detection using the Sobel operator on the image. This gives an image containing thick edges with a wide range of intensities which need to be thinned and thresholded to detect the meaningful edges. For this step, we use the method of edge drawing based on Topal and Akinlar [13], resulting in a binary image only including thin edges. Besides the edges separating land and sea, many edges are present on land because of the high contrast of buildings, fields, and roads. Some edges are also present in the water, following wind or current structures which show brightness differences in SAR images. The muddy land areas are also found because they are darker than the water and their edges are mostly strong enough for detection.

To differentiate between land and sea, a binary landmark based on data from the Shuttle Radar Topography Mission (SRTM) Water Body Database (SWBD) is generated for the respective scene. Then, a flood fill algorithm is run on the binary edge image; this standard type of algorithm finds all points connected to and having the same value as a given starting point. We use all image corners where the SRTM landmark suggests water as starting points and let the flooding extend to 4-connected neighbours only, as many diagonal

lines are produced by the edge drawing which would not stop the flooding if 8-connectivity was used. The flood filling will stop at the contours of the edge image, marking all reached pixels including the contours as water. All pixels not reached by the flood are thereafter considered to be land. Hence, with this method only the sea-land-boundary is detected; inner lakes not reached by the flood fill algorithm are marked as land. As edge points are also marked as water, isolated edges reached by the flood (like single wave lines in the open sea) are automatically removed. The result of this step is a first binary mask showing land and water area, which is further refined in the following steps.

The edge drawing algorithm requires the setting of two thresholds for edge values to follow: an upper threshold to determine strong edges as contour starting points and a lower threshold to determine the minimum edge strength to still be considered a valid edge (as opposed to noise). In case of too high thresholds, important edges are ignored and the flood extends to large parts of the mainland; for too low thresholds, many edges in the water are traced and large parts of the sea are marked as land. However, the optimal threshold values were found to be different for each scene, depending on illumination parameters as well as ground parameters like sea state.

As an automatic method to set these thresholds as good as possible, a brightness landmask is generated from the smoothed image using Otsu's method [14] for histogram-based thresholding of the entire scene. While this does not cover mud flats which are darker than the water, the mainland and dry sands are usually very well covered. This is also why this landmask yields better results than the SRTM mask which especially for low tides does not cover the many bright sand areas. The generated flood fill landmask is then compared to the brightness landmask, yielding an agreement value based on how many of the pixels are identical. In the next step, the SRTM data is used to modify this agreement value. From the original SRTM landmask, a landmask with eroded land is generated, indicating safe land pixels but taking into account possible imprecisions in the SRTM data due to the ongoing changes in the shape and position of islands. A penalty is subtracted from the agreement value for pixels, where the eroded SRTM landmask indicates land but the flood fill landmask does not.

The iteration consists of the steps of edge drawing, flood filling, and determination of the agreement value. With starting parameters of $T_{u,s} = 0.12$ for the upper and $T_{l,s} = 0.03$ for the lower threshold (where 1.0 equals the highest edge strength in the image), the iteration steps are performed, yielding an initial agreement value. These starting thresholds were found to be the average of many scenes. A hill climbing approach is used to determine the optimal thresholds yielding the highest agreement value. The current thresholds (T_u, T_l) are increased or decreased by ($\Delta T_u = 0.005, \Delta T_l = 0.0025$) and the iteration steps are performed with these new thresholds. If a higher agreement value is found, the corresponding thresholds are then used as new starting parameters for the next iteration. The hill climbing terminates if no combination of ($T_u \pm \Delta T_u, T_l \pm \Delta T_l$) is found that yields a higher agreement

value. This usually requires 10–30 iterations of the edge drawing and flooding procedures.

When the landmask was generated using the determined best threshold values, all islands smaller than 5 pixels are removed from the landmask. Particularly for pronounced wave crests, many edges are found which are tracked because their strength is comparable to true land-water-boundaries. Due to the flooding algorithm described above, only edges that form closed boundaries produce misdetected islands. These often consist of only one or very few pixels, similar to ships and small stationary structures like buoys which are detected as land due to the very high contrast and the resulting high edge values. Removing these small pseudoislands greatly improves the resulting landmask.

The final output of the algorithm is a binary landmask, created with the determined best thresholds for edge drawing and with small land objects removed, allowing a differentiation of land and sea unique to the respective SAR scene.

Note that the availability of SRTM data is helpful for the algorithm, but not mandatory. Without these data, the starting points for flood filling are taken from the brightness landmask, which is more prone to error as bright sea areas in near range may be detected as land and no starting point can be found. During calculation of the agreement value, the subtraction of the penalty is then skipped, making solutions where larger parts of the land are flooded more likely.

3. Results

The algorithm was applied to several TS-X Stripmap and ScanSAR scenes of the Wadden Sea. Two exemplary results are presented in Figures 3 and 4; Figure 2 gives an overview of the area. Acquisition details of the scene are given in Table 1.

3.1. Scene A: Trischen. In Figure 3, a subsection of the area between island Trischen (in the upper left) and the mainland near Friedrichskoog is shown, taken from a TS-X Stripmap scene from December 2013, recorded during low tide. South of Trischen, the sand bank Mittelplate, is located, where the largest offshore oil rig in Germany is visible as bright, rectangular area. Note the large variation of the NRCS in the tidal mudflats, showing many areas with very high and very low backscatter directly adjacent to each other. The range of intensities is even higher than in the agricultural area of the mainland with the rectangular structures telling their human origin. The grasslands in the coastal areas of the mainland and on Trischen, in contrast, show a very homogeneous grey level. The comparison between the SRTM measurements of the coastline recorded in 2000, shown in blue, and the current position and extension of Trischen easily visible in the TS-X scene indicates the dynamics of the Wadden Sea islands and sand banks. This difference is almost nonexistent at the mainland coast protected by dikes and coastal protection measures. The green lines show our algorithm's result. Most areas with mud flats are correctly identified and many small tidal inlets are found, although they are no longer captured when they become too narrow. This is caused by the median

TABLE 1: Acquisition parameters for the presented TS-X scenes. The scenes were acquired in Stripmap (SM) and ScanSAR (SC) mode, respectively.

Scene	Mode	Acquisition date	Pol.	Incidence angle	Pixel size
A: Trischen	SM	2013-12-13	VV	29.6–32.5°	2.75 m × 2.75 m
B: Pellworm	SC	2013-11-12	VV	38.1–45.6°	8.25 m × 8.25 m

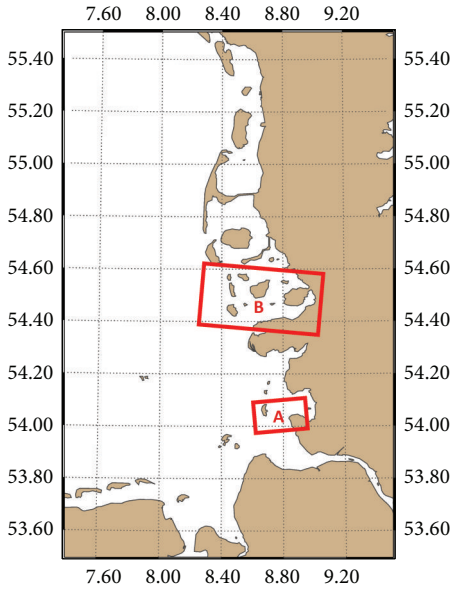


FIGURE 2: Overview of the study area in the Wadden Sea. Our results for the areas marked A and B are shown in Figures 3 and 4, respectively.

smoothing which removes structures smaller than the filter size. The sand bank Mittelplate is split up into several parts by our algorithm where the human eye would draw a single connected area. This is caused by the low contrast present in many parts of its edges; hence, some of the interior parts are reached by the flood fill algorithm and marked as water.

3.2. Scene B: Pellworm. Figure 4 shows a subsection of a TS-X ScanSAR scene, showing island Pellworm and surroundings in a high tide situation. On the left hand side of the image, the three sand banks Japsand, Norderoogsand, and Süderoogsand (from top to bottom) are seen as dark areas while the grass-covered island Hooe east of Japsand appears brighter than the sea. Similar to Trischen discussed above, these sand banks have apparently changed since the SRTM mission, as the SRTM landmask shows different outlines for all these banks when compared to the scene directly and also with our algorithm. At the top right of Figure 4, the blue SRTM landmask shows the contours of several inland water bodies, which our algorithm does not detect because they are not connected to the sea, and the same yields true also for two smaller lakes in the mainland at the bottom part of Figure 4. Following the mainland to the bottom of the image, another sand bank, Westerheversand, is shown as being connected to the mainland in the SRTM landmask. However, at the time of recording it is apparently separated, which is also reflected by

the results of our algorithm. Similarly, above this sand bank is a location where the SRTM landmask reports a small land structure which is not visible in the TS-X scene, either due to high tidal state or changes in the topography. In the top left of Figure 4, a single misdetection of our algorithm is seen, where strong wave structures were traced and ended up forming a closed pattern. As this extends the minimum size for deletion, which, as clearly seen in other parts of the scene, may not be strongly increased due to several small islands, this currently cannot be completely avoided. The mainland coastline in the lower part of the image also shows some coarse structures produced by our algorithm where it followed wave structures into the sea. Nevertheless, the coastline is represented very well on average.

3.3. Runtime. As a short computation time is crucial for NRT processing, this section presents the algorithm's run-times. These times were measured on a notebook PC with an Intel(R)Core(TM)2 Extreme Q9300 CPU running at 2.53 GHz with 2 GB of RAM available. The processing was performed with the scenes downsampled by a factor of 4 which is commonly used also for other value adding marine SAR products. The results are given in Table 2. As both scenes have almost the same total number of pixels (≈ 15 Mil.), times for the individual steps do not differ much; for both scenes, the two smoothing steps take 13 s each while creating the brightness landmask takes 5 s. One iteration step, which consists of edge drawing, flood filling, and agreement value calculation, takes 5 s for the Trischen scene but 6 s for the Pellworm scene as it contains more water to be filled.

4. Discussion

The described algorithm is able to detect the land-waterline to a high level of accuracy. Despite the challenging conditions in the Wadden Sea area involving many dark mudflats, the adapted edge detection and edge drawing algorithms were able to follow most of the boundaries. As only a low amount of edge-preserving smoothing is used, the detected edges are usually not shifted compared to those observed by visual observation. This also allows the algorithm to better track small inlets like tidal creeks often present at low tide in the Wadden Sea. Although developed with data of the Wadden Sea, the algorithm can of course also be applied to SAR data of other tidal mudflat areas or of coastal areas in general.

An advantage of this algorithm is its fast operation, allowing for an application under Near Real Time (NRT) demands as the processing takes only a few minutes for a full TS-X scene. The generated landmask can then be used for further processing of other maritime SAR products like wind field estimation, wave height retrieval, or ship detection.

TABLE 2: Runtime for the two presented acquisitions. The number of iterations indicates how many threshold pairs were evaluated during the iterative steps; $(T_{u,b}, T_{l,b})$ gives the best threshold pair found.

Scene	Pixel dimensions	Iterations	$(T_{u,b}, T_{l,b})$	Runtime
A: Trischen	2917 × 5136	17	(0.16, 0.0375)	191 s
B: Pellworm	3183 × 4692	21	(0.15, 0.0150)	241 s

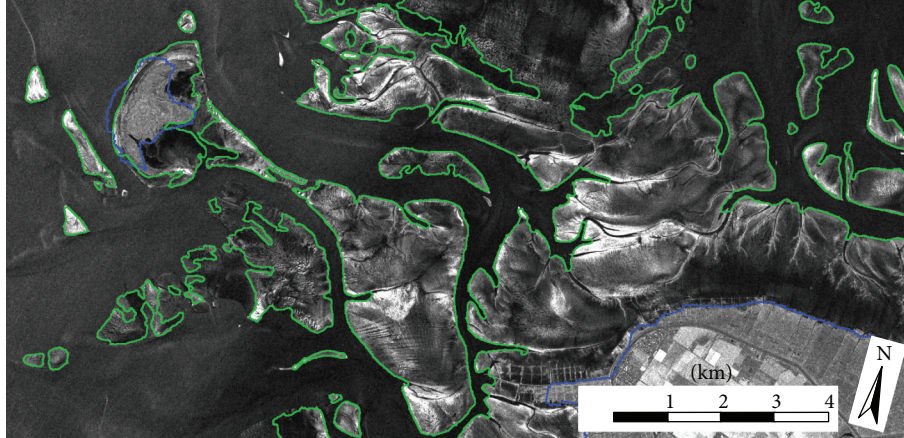


FIGURE 3: The algorithm's results overlaid on the original image. The green lines show the sea-land-boundaries from our algorithm while the blue lines show the sea-land-boundaries from the SRTM landmask. This subsection of a low tide TS-X Stripmap scene shows the island Trischen in the upper left and the mainland with the city of Friedrichskoog in the bottom right. During this low tide scene, our algorithm clearly shows the extension of the mud lands and sand banks.

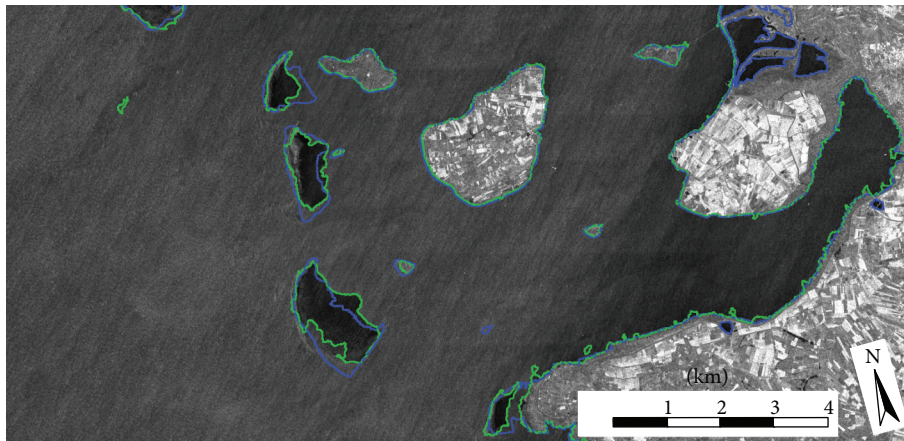


FIGURE 4: The algorithm's results overlaid on the original image. The green lines show the sea-land-boundaries from our algorithm while the blue lines show the sea-land-boundaries from the SRTM landmask. This subsection of a high tide TS-X ScanSAR scene from November 2013 shows the area around the island Pellworm (middle) with sand banks and smaller islands. Our algorithm traces the contours of sand banks, islands, and mainland alike.

These products are dependent on an accurate landmask to avoid wrong calculations and misdetections due to unmasked land. In the Wadden Sea, common datasets like SRTM do not cover the low tide situations and their accuracy, as seen in Figures 3 and 4, is quickly deprecating due to constant changes of island and sand bank topography. Also, our algorithm is well suited to support these products as it is independent of polarimetric or interferometric acquisitions.

The algorithm depends on optimally set threshold values determined by the comparison between the current flood filling landmask, the brightness landmask, and the SRTM landmask. A depth map of the southeastern North Sea could

be used to act as an additional comparative landmask and also to filter out unwanted island-like detections caused by wave structures or large ships in deep water. In some parts, a transition between water and land is visible to the human eye due to texture changes where hardly any brightness change occurs; hence, such a transition is not detected by the edge detector. Texture based methods for detecting these boundaries may improve the detection accuracy in a future version.

Data from the TS-X mission provide a large coverage of the Wadden Sea area and are frequently available with a repetition time of 11 days for the same orbit. Using data

from several acquisitions, the evolution of sand banks and coastlines can be monitored. Additionally, as the acquisitions will contain different tidal levels, a combination of the retrieved waterlines and in situ tidal gauge data will permit a reconstruction of the bathymetry, similar to the methods used by [11, 12]. We aim to present these studies in a future publication.

Conflict of Interests

The authors declare that there is no conflict of interests regarding the publication of this paper.

Acknowledgment

The TS-X data were kindly provided by DLR via Proposal OCE2738.

References

- [1] G. Herrling and C. Winter, "Morphological and sedimentological response of a mixed-energy barrier island tidal inlet to storm and fair-weather conditions," *Earth Surface Dynamics*, vol. 2, no. 1, pp. 363–382, 2014.
- [2] X.-M. Li and S. Lehner, "Algorithm for sea surface wind retrieval from TerraSAR-X and TanDEM-X data," *IEEE Transactions on Geoscience and Remote Sensing*, vol. 52, no. 5, pp. 2928–2939, 2014.
- [3] D. van der Wal, P. M. J. Herman, and A. W.-V. den Dool, "Characterisation of surface roughness and sediment texture of intertidal flats using ERS SAR imagery," *Remote Sensing of Environment*, vol. 98, no. 1, pp. 96–109, 2005.
- [4] J.-S. Lee and I. Jurkevich, "Coastline detection and tracing in SAR images," *IEEE Transactions on Geoscience and Remote Sensing*, vol. 28, no. 4, pp. 662–668, 1990.
- [5] H. Liu and K. C. Jezek, "Automated extraction of coastline from satellite imagery by integrating Canny edge detection and locally adaptive thresholding methods," *International Journal of Remote Sensing*, vol. 25, no. 5, pp. 937–958, 2004.
- [6] U. Acar, B. Bayram, F. B. Sanli, S. Abdikan, F. Sunar, and H. I. Cetin, "An algorithm for coastline detection using SAR images," *International Archives of the Photogrammetry, Remote Sensing and Spatial Information Sciences*, vol. XXXIX-B3, pp. 457–460, 2012.
- [7] Y. Yu and S. T. Acton, "Automated delineation of coastline from polarimetric SAR imagery," *International Journal of Remote Sensing*, vol. 25, no. 17, pp. 3423–3438, 2004.
- [8] S. Dellepiane, R. De Laurentiis, and F. Giordano, "Coastline extraction from SAR images and a method for the evaluation of the coastline precision," *Pattern Recognition Letters*, vol. 25, no. 13, pp. 1461–1470, 2004.
- [9] M. Gade, S. Melchionna, K. Stelzer, and J. Kohlus, "Multi-frequency SAR data help improving the monitoring of intertidal flats on the German North Sea coast," *Estuarine, Coastal and Shelf Science*, vol. 140, pp. 32–42, 2014.
- [10] D. C. Mason and L. J. Davenport, "Accurate and efficient determination of the shoreline in ERS-1 SAR images," *IEEE Transactions on Geoscience and Remote Sensing*, vol. 34, no. 5, pp. 1243–1253, 1996.
- [11] A. Niedermeier, D. Hoja, and S. Lehner, "Topography and morphodynamics in the German Bight using SAR and optical remote sensing data," *Ocean Dynamics*, vol. 55, no. 2, pp. 100–109, 2005.
- [12] G. Heygster, J. Dannenberg, and J. Notholt, "Topographic mapping of the German tidal flats analyzing SAR images with the waterline method," *IEEE Transactions on Geoscience and Remote Sensing*, vol. 48, no. 3, pp. 1019–1030, 2010.
- [13] C. Topal and C. Akinlar, "Edge drawing: a combined real-time edge and segment detector," *Journal of Visual Communication and Image Representation*, vol. 23, no. 6, pp. 862–872, 2012.
- [14] N. Otsu, "A threshold selection method from gray-level histograms," *IEEE Transactions on Systems, Man and Cybernetics*, vol. 9, no. 1, pp. 62–66, Jan 1979.



Hindawi

Submit your manuscripts at
<http://www.hindawi.com>

